The use of concentrated solar energy to weaken rocks and reduce their grinding energy

Hassan Alsaraj, Dr. Ali Alkadhem, Prof. Bassam Dally

hassan.alsaraj@kaust.edu.sa, Ali.Alkadhem@kaust.edu.sa, bassam.dally@kaust.edu.sa

Abstract

Comminution, the crushing and grinding of ore, accounts for 30–50% of a mining operation's total energy consumption, a burden that keeps growing as high-grade deposits are depleted. Thermal shock pretreatment can weaken rock before milling, but conventional approaches rely on carbon-intensive furnaces that erode the net energy benefit. This report investigates concentrated solar energy as a zero-carbon alternative: a high-flux solar simulator rapidly heated 20 g gold-ore samples to 600, 700, and 800 °C for 2.5, 5, and 7.5 min, after which grindability was assessed via particle size distribution, the Bond Work Index (Wi), and XRF/XRD characterization. Mass loss increased with temperature, reaching up to 16.7% at 800 °C, consistent with carbonate decomposition and chlorite dehydroxylation. Grindability improved most at 700–800 °C, and the Bond Work Index at 800 °C fell from 558 kWh/ton at 2.5 min to 167 kWh/ton at longer exposure, a reduction of nearly 70% relative to the raw sample's 514 kWh/ton. These results show that solar-driven thermal shock can reproduce the comminution-energy savings of furnace-based thermal shock, while replacing grid electricity with a renewable heat source.

[date]**Date:** August 24, 2026

In partnership with

Contents

1 Introduction 2

2 Related Work 2

3 Methodology 3

3.1 Method details . . . 3

3.2 Evaluation Procedure . . . 4

4 Results 7

5 Discussion 15

6 Limitations and Future Work 17

7 Conclusion 18

Acknowledgments 18

References 18

1 Introduction

Extracting valuable minerals such as gold relies heavily on comminution, the crushing and grinding of ore. This stage is energy-intensive, accounting for 30 to 50 percent of a mining operation's total energy consumption [1]. As high-grade deposits become scarce, the industry must process harder, lower-grade ores, driving up grinding times, energy demands, and operational costs. Researchers are therefore exploring pretreatment technologies that structurally weaken the rock before milling, reducing the mechanical energy required for size reduction [2].

Thermal shock treatment is a highly effective pre-weakening strategy. When ore is subjected to sudden, intense heat, the varying thermal expansion rates of its minerals create severe internal stresses along the thermal gradient. In gold ores containing carbonate or hydrated minerals, this heat also triggers chemical breakdowns, such as carbonate decomposition releasing carbon dioxide [3], which forces the material to fracture from the inside out. However, traditional thermal shock experiments rely on electric or gas furnaces, where heat reaches the ore mainly through heat conduction and convection from the furnace walls. Relying on these carbon-intensive heat sources can offset the environmental and economic benefits of saving grinding energy.

To close this gap and address the need for a sustainable pretreatment method, this study investigates concentrated solar energy, delivered by heat radiation, to induce thermal shock in gold ore. A calibrated solar simulator subjected representative gold ore samples to rapid, high-flux radiative heating to trigger internal microcracking and structural degradation. By analyzing thermal mass loss and post-treatment grinding efficiency, this report assesses the viability of solar thermal pretreatment as a zero-carbon strategy to optimize comminution.

2 Related Work

Several studies have used heat to make ore easier to grind, since grinding consumes a large share of total energy in mineral processing [1, 2]. Fast heating, called thermal shock, makes different minerals expand at different speeds due to their differing thermal expansion coefficients. Under a steep thermal gradient, this differential expansion generates stresses that exceed the rock's local fracture strength, producing microcracks along grain boundaries. In carbonate-bearing ores, heat also breaks down carbonates and releases gas, adding further cracking [3].

In furnace-based thermal shock studies, heat is delivered primarily by heat conduction: the sample sits in contact with, or surrounded by, resistively heated furnace walls, and thermal energy diffuses into the rock down a conductive gradient. This is how nearly all prior thermal shock literature has delivered heat; the present study is not a comparison of two competing heating methods, but an extension of this research to a heat-transfer pathway, radiative heating, not yet characterized for thermal shock pretreatment of gold ore.

The study most similar to this one is by Ababneh, Lopez Aguirre, Alkadhem, and Dally (2026), titled "Reducing Comminution Energy of Gold Ores Through Thermal Shock Treatment" [4]. Like this report, they treated gold ore with fast heating between 500 and 800 °C for short times (0.5 to 10 min), ground the ore, and used the Bond Work Index to measure grinding energy saved. They found that heating below 700 °C gave little benefit, while 700–800 °C for 1–5 min gave the best results, cutting grinding energy by up to about 50%. This study follows a similar method: the same 20 g sample mass, the same ball mill, and similar treatment temperatures (600–800 °C) and times (2.5–7.5 min), so the two sets of results can be compared.

Ababneh et al. (2026) heated their samples in an electric tube furnace, a conduction/convection-driven process running on grid electricity. This study instead delivers thermal shock by heat radiation: concentrated, high-flux radiative heating directly at the sample surface, reproducing

the radiative heat transfer of concentrated sunlight under controlled lab conditions. This is the gap the present work aims to close: whether a purely radiative heat-transfer pathway can reproduce the grindability improvements previously reported for furnace heating, using a heat source independent of grid electricity. The longer-term goal is to use real sunlight, focused with mirrors or lenses, to heat the ore at a mine site.

3 Methodology

3.1 Method details

Materials and Equipment

A 0.5 kg bulk sample of crushed gold ore was used. The sample was sieved to the 2000–4000 μm size range using ASTM-standard sieves and divided into 20 g portions, so that every treatment condition started from the same amount of material.

The following equipment was utilized:

- **Thermal shock treatment:** An HFSS-7-42 high-flux solar simulator was used to heat the samples quickly to the target temperature. Each 20 g sample was placed in a glass tube at the focal point of the simulator.

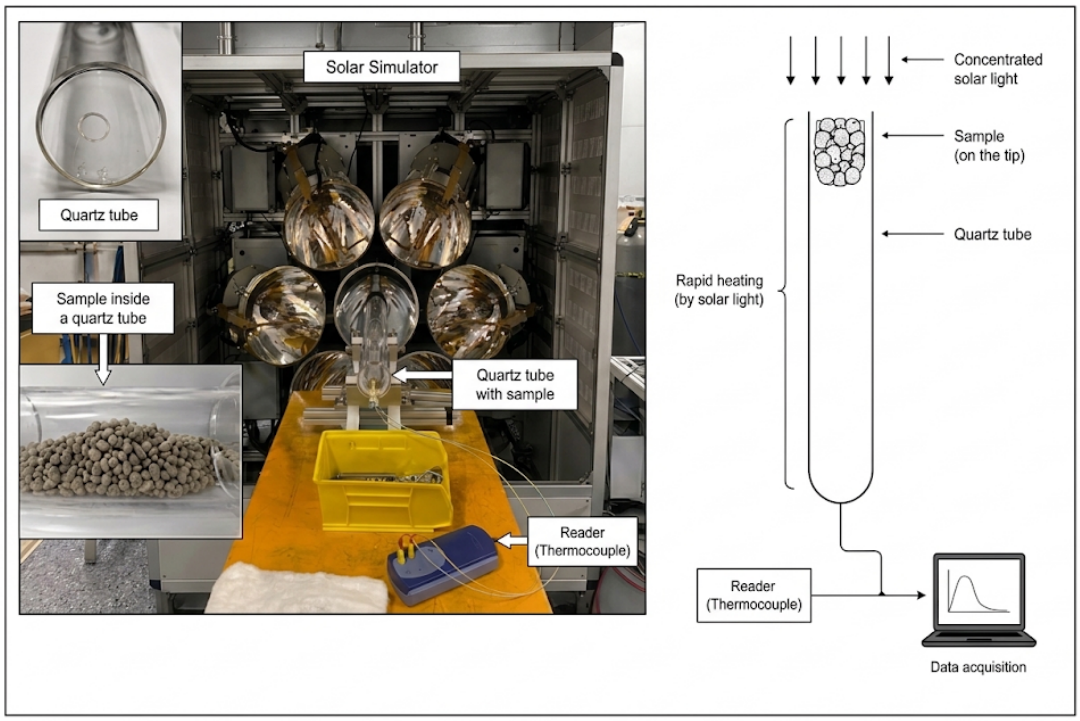


Figure 1 The HFSS-7-42 high-flux solar simulator used for thermal shock treatment of the ore samples (left), and a schematic of the setup showing how concentrated solar light heats the sample inside the quartz tube, with a thermocouple reader logging temperature to a data acquisition computer (right).

- **Ball mill (grinding):** Grinding was done using a Retsch PM200 planetary ball mill, which rotates in alternating directions to grind the sample evenly.

Thermal shock treatment

Each 20 g sample was placed at the focal point of the solar simulator, where it received concentrated, high-flux heat radiation from an array of xenon short-arc lamps. This radiative path



Figure 2 The Retsch PM200 planetary ball mill used to grind the samples before and after thermal treatment.

delivers thermal energy directly to the ore surface, so the resulting internal thermal gradient and stresses are driven by the incident radiative flux. To create a real thermal shock, the simulator first ran at high power (15,000 W) to quickly heat the sample. Once the sample reached the target temperature range, power was lowered to the calibrated value needed to hold that temperature (600, 700, or 800 °C) for the set exposure time (2.5, 5, or 7.5 min). The initial fast-heating step was not counted as part of the exposure time; only the time held at the target temperature was counted.

After treatment, the simulator was switched off and the sample cooled for 10 min before weighing and further handling.

Determining the steady-state grinding time

Before comparing treated and untreated samples, it was necessary to find a grinding time long enough that further grinding would not change the particle size much. This is called the steady-state grinding time. To find this, samples were ground for several different times, then sieved, and the particle size at which 80% of the material passes (D80) was plotted against grinding time.

Once the D80 value stopped decreasing significantly with more grinding time, that grinding time was chosen as the fixed grinding time used for every sample in this study, so that treated and untreated samples could be compared fairly.

Grinding

Every 20 g sample, treated and untreated, was ground for the same, fixed time using the Retsch PM200 ball mill. The direction of rotation was reversed partway through the grinding cycle to help grind the sample evenly, and a counterweight was used to keep the mill balanced.

3.2 Evaluation Procedure

Particle size distribution (PSD) analysis

ASTM-standard sieves (Humboldt Manufacturing) were used to separate the ground samples into different particle size ranges by dry sieving. After grinding, each sample was dry-sieved through a stack of standard sieves (2000, 850, 600, 425, 250, 125, and 75 μm), and the mass retained on each sieve was recorded. This was used to build a cumulative passing curve (the

percentage of the sample finer than each sieve size) for every treatment condition, and to compare it to the untreated raw sample.



Figure 3 Standard sieve set used for particle size distribution analysis.

Mass and Chemical Characterization

Samples were weighed before and after treatment, and before and after grinding, using a laboratory balance.

A small subsample (0.3 g) was taken from each treated bulk sample and from the untreated raw sample. Each subsample was ground to a fine powder by hand and analyzed by an X-ray fluorescence (XRF) spectrometer to check for changes in chemical composition caused by the thermal treatment.

Crystallographic Analysis (XRD)

A Bruker D2 Phaser X-ray diffraction (XRD) instrument collected sample crystallographic data. XRD identifies mineralogical phase transformations and confirms the microcracking induced by the thermal gradients.

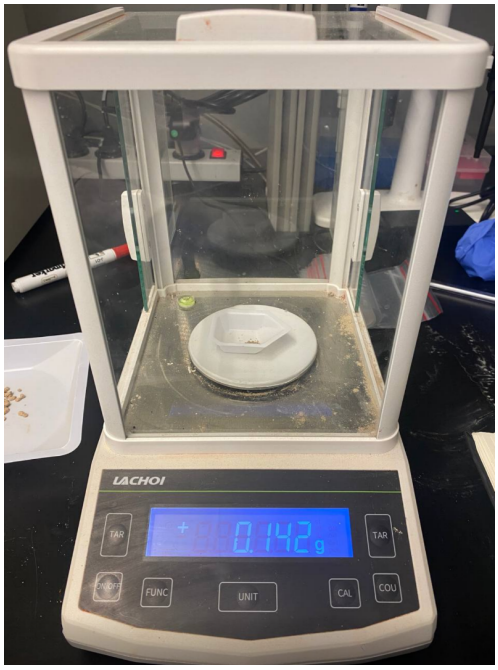


Figure 4 Balance used to record sample mass throughout the experiment.



Figure 5 XRF spectrometer used for elemental composition analysis of the ore samples.

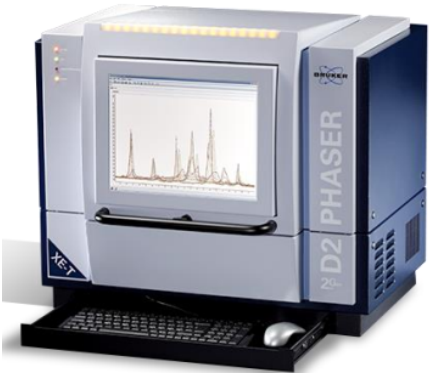


Figure 6 XRD Bruker D2 Phaser instrument employed to collect sample crystallographic data.

4 Results

Thermal decomposition behavior of the raw ore

Figure 7a shows a thermogravimetric (TGA) weight-loss profile of the raw ore, included to give a slow-heating reference point for the treatment window used in this study. The sample stays essentially flat up to about 580 °C, then loses roughly 10% of its weight in a first, sharp step between about 580 and 700 °C, before a second, more gradual step brings the total loss to around 17–18% by 850 °C, after which the curve plateaus. This staged behavior is consistent with sequential decomposition of the magnesite and dolomite identified by XRD, and dehydroxylation of chlorite [4, 3]. It also brackets the 600–800 °C window used for the thermal shock treatments below: 600 °C sits just above the onset of decomposition, while 700–800 °C spans the temperatures where the bulk of the accessible mass loss occurs under slow heating.

Mass loss under thermal shock

The mass of each sample was measured before and after thermal treatment. Table 1 and Figure 7b show the percentage of mass lost for each temperature and exposure time. Averaged over exposure time, mass loss rises with temperature, from 11.7% at 600 °C to 13.3% at 700 °C and 16.7% at 800 °C, consistent with progressively more complete decomposition of the carbonate phases and release of CO_2 [3]. At 800 °C, mass loss is highest at 2.5 and 5 min (17.5% each) and slightly lower at 7.5 min (15.0%), suggesting that most of the decomposition reactions are already complete within the first few minutes of exposure at this temperature. Notably, the 16.7% average mass loss reached at 800 °C after only a few minutes of solar thermal shock is already close to the ∼17–18% total loss the TGA curve only reaches after slow heating all the way to 850 °C, indicating that rapid radiative heating accesses most of the same decomposition chemistry in a small fraction of the time.

Table 1 Mass loss (%) after thermal shock treatment.

Time (min)	600 °C	700 °C	800 °C
2.5	12.5	12.5	17.5
5	10.0	12.5	17.5
7.5	12.5	15.0	15.0
Average	11.67	13.33	16.67

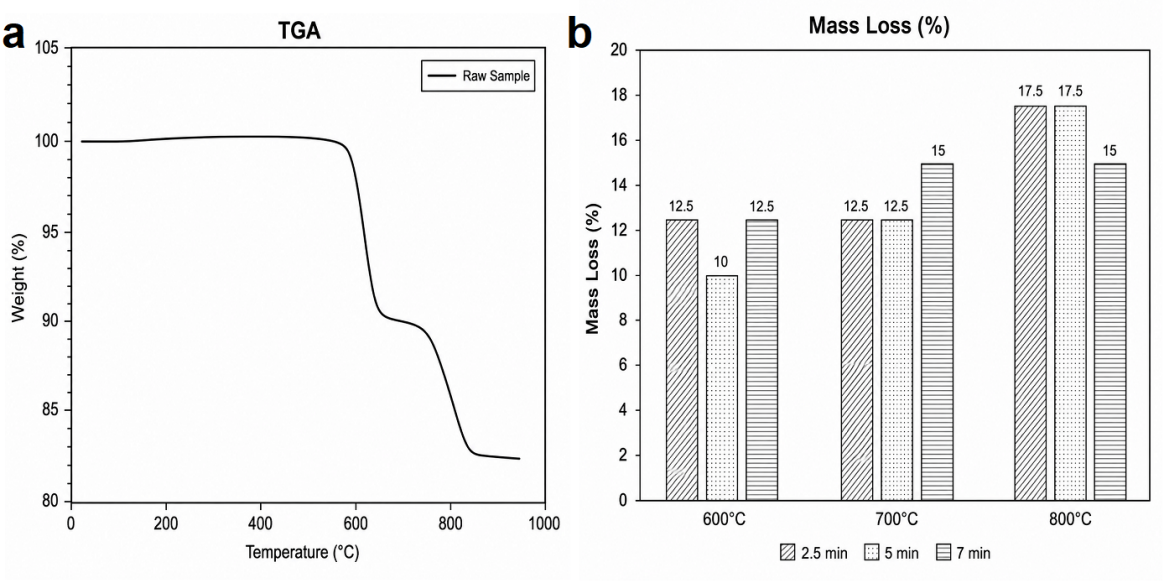


Figure 7 (a) Thermogravimetric (TGA) weight-loss profile of the raw ore under slow heating, shown for context. (b) Mass loss (%) of samples treated at 600 °C, 700 °C, and 800 °C for 2.5, 5, and 7 min.

Particle size distribution after grinding: 600 °C samples

Figure 8 compares the raw (untreated) sample with samples treated at 600 °C for 2.5, 5, and 7.5 min.

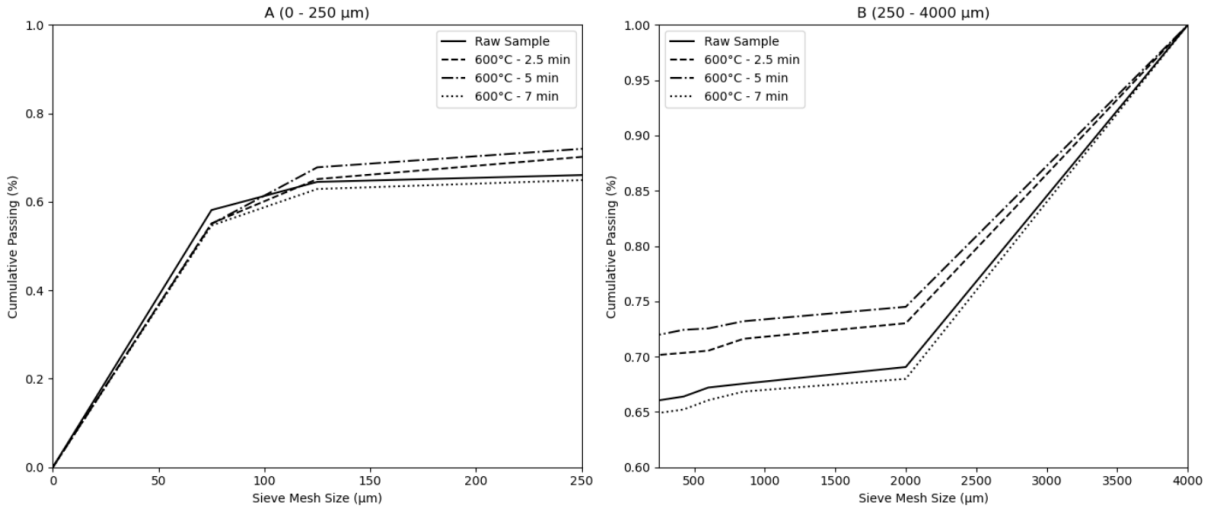


Figure 8 Particle size distribution (cumulative passing vs. sieve mesh size) for the raw sample and samples treated at 600 °C for 2.5, 5, and 7.5 min. (A) 0–250 μm range. (B) 250–4000 μm range.

700 °C samples

Figure 9 compares the raw sample with samples treated at 700 °C for 2.5, 5, and 7.5 min.

800 °C samples

Figure 10 compares the raw sample with samples treated at 800 °C for 2.5, 5, and 7.5 min.

XRD phase evolution

To see which minerals were being broken down by the heat, the crushed samples were analyzed by X-ray diffraction (XRD) before and after treatment. Figures 11, 12, and 13 compare the

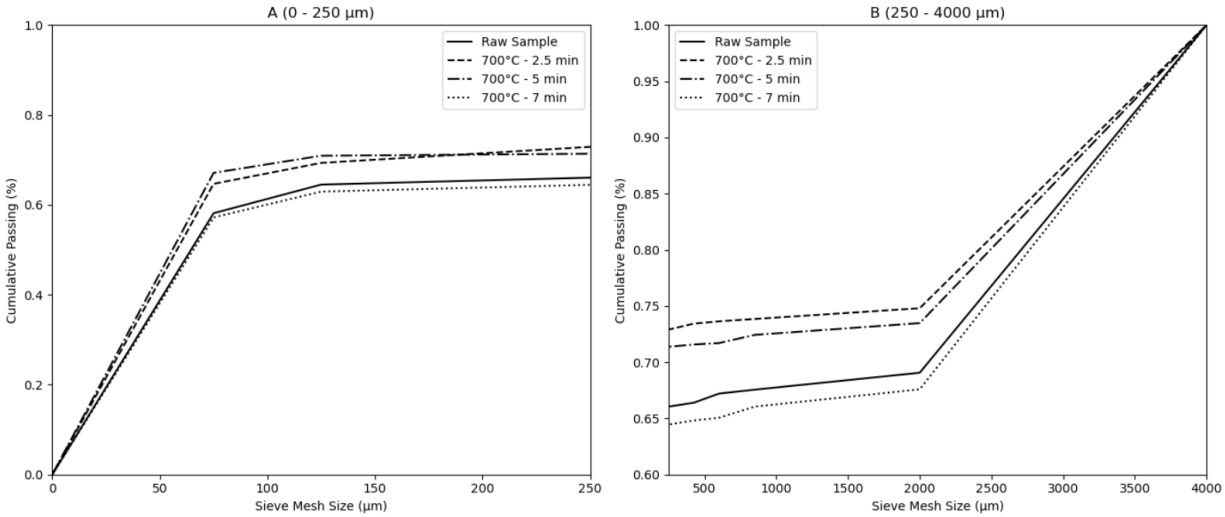


Figure 9 Particle size distribution (cumulative passing vs. sieve mesh size) for the raw sample and samples treated at 700 °C for 2.5, 5, and 7.5 min. (A) 0–250 μm range. (B) 250–4000 μm range.

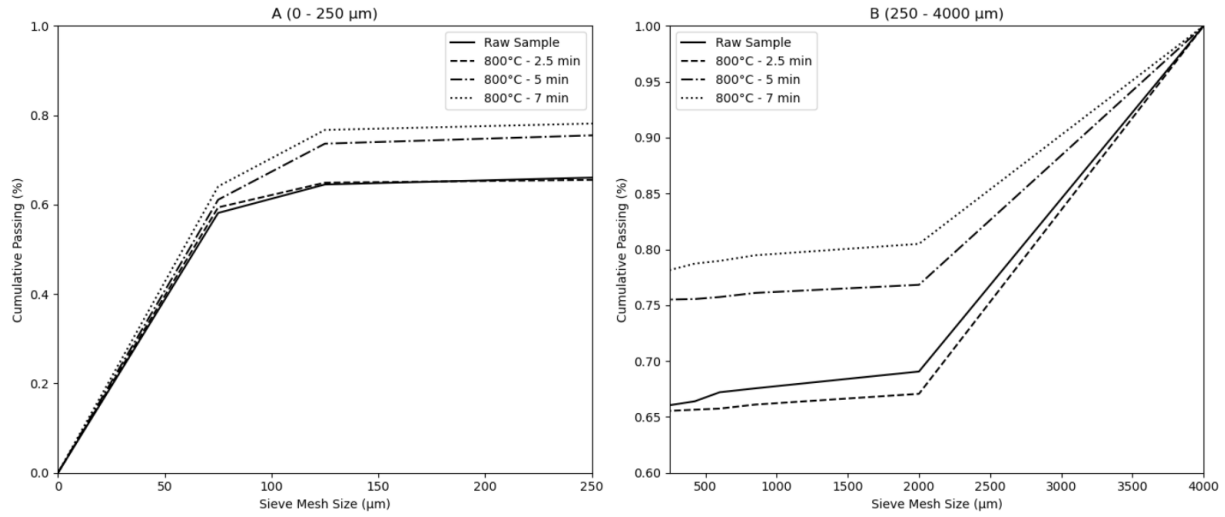


Figure 10 Particle size distribution (cumulative passing vs. sieve mesh size) for the raw sample and samples treated at 800 °C for 2.5, 5, and 7.5 min. (A) 0–250 μm range. (B) 250–4000 μm range.

raw sample's diffraction pattern with samples treated at 600, 700, and 800 °C. The main phases identified are quartz, chlorite, magnesite, muscovite, and dolomite, consistent with the mixed silicate-carbonate mineralogy expected for this ore [4].

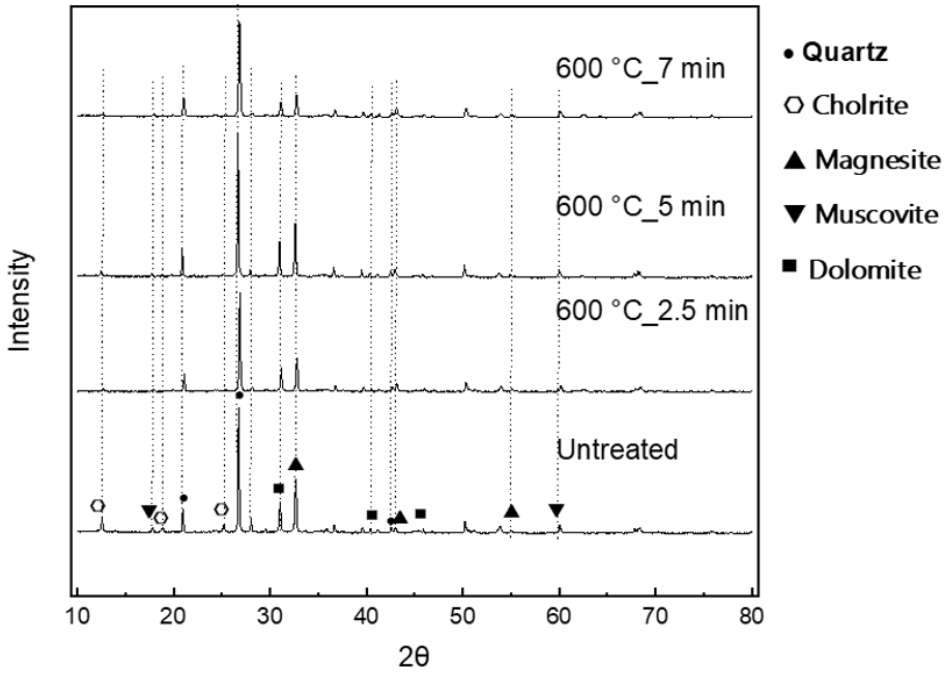


Figure 11 XRD pattern of the raw sample compared with samples treated at 600 °C for 2.5, 5, and 7 min.

At 600 °C (Figure 11), the diffraction pattern changes only slightly from the raw sample at all three exposure times. The main quartz peak stays roughly the same height, and the dolomite and magnesite peaks show only a small reduction in intensity. This matches the mass-loss and BET data, which also showed only a modest, inconsistent effect at this temperature, and suggests that 600 °C is not hot enough to decompose much of the carbonate in the ore.

At 700 °C (Figure 12), the carbonate peaks from magnesite and dolomite are visibly weaker than in the raw sample, particularly at 5 and 7 min, indicating that these carbonate minerals are starting to decompose into oxide phases. The chlorite peaks also lose intensity, consistent with the onset of dehydroxylation. This tracks the sharp increase in mass loss and specific surface area already seen at 700 °C.

At 800 °C (Figure 13), the change is the most dramatic: the magnesite and dolomite peaks are strongly suppressed by 5 and 7 min, meaning most of the carbonate in the sample has broken down into oxide phases such as periclase, MgO. The quartz peak stays strong throughout, since quartz does not decompose in this temperature range; it only undergoes a reversible phase transition near 573 °C that is not detectable once the sample has cooled back to room temperature [4]. This pattern is consistent with the near-complete carbonate breakdown inferred from the mass-loss data at 800 °C, and it supports the same explanation used for the chemical composition trends in Table 2: MgO content rises and the carbonate character of the ore is progressively lost as treatment severity increases.

Chemical composition

Table 2 shows the XRF results for the raw sample and for samples treated at 600, 700, and 800 °C for different exposure times.

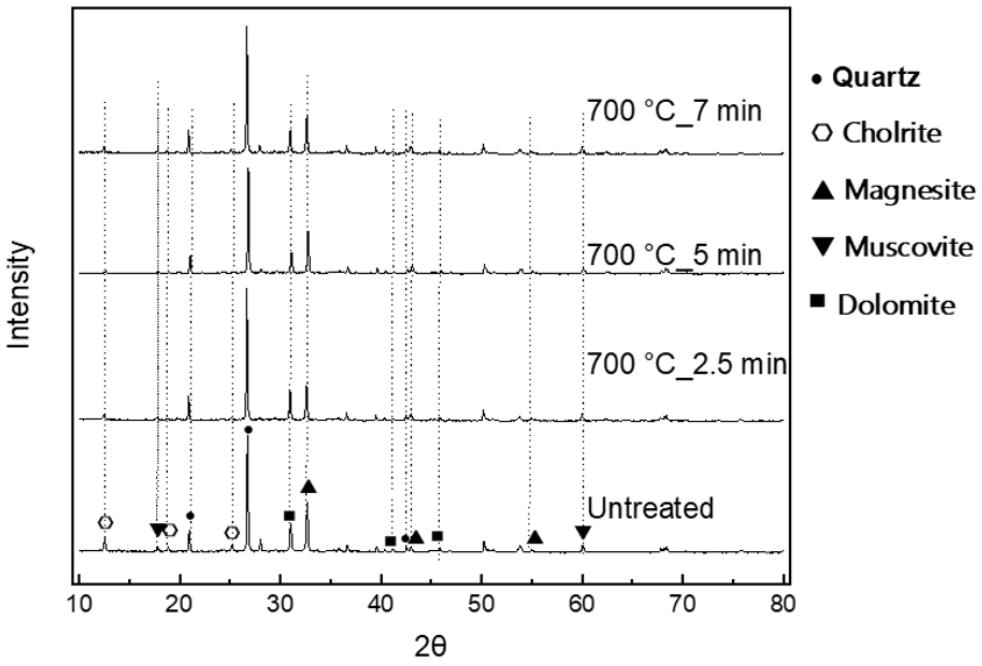


Figure 12 XRD pattern of the raw sample compared with samples treated at 700 °C for 2.5, 5, and 7 min.

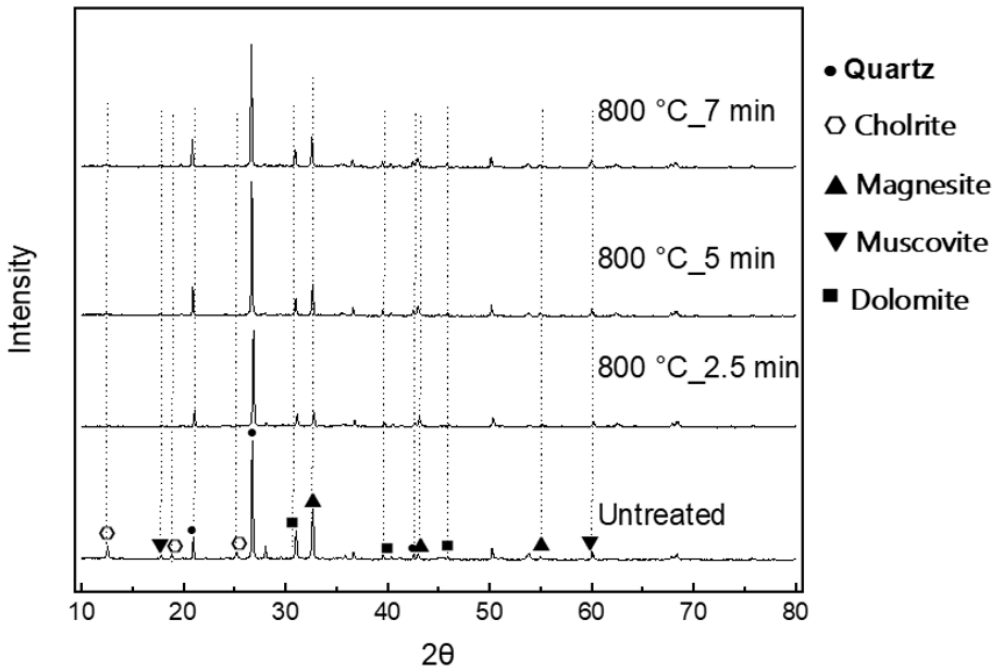


Figure 13 XRD pattern of the raw sample compared with samples treated at 800 °C for 2.5, 5, and 7 min.

Table 2 XRF analysis results for the raw sample and treated samples.

Temp. (°C)	Time (min)	SiO_2	MgO	CaO	Fe_2O_3	Al_2O_3	SO_3
Raw	–	46.0	13.3	5.73	8.579	8.31	0.638
600	2.5	43.1	15.8	6.24	8.451	8.00	0.804
600	5	44.7	15.4	6.12	8.522	7.54	0.771
600	7	48.0	17.7	5.90	7.811	7.40	0.922
700	2.5	45.4	15.9	7.06	8.489	7.69	0.619
700	5	42.5	16.4	6.36	8.456	6.87	0.926
700	7	44.4	15.8	5.29	8.647	7.20	0.793
800	2.5	47.3	18.6	6.17	8.765	7.49	0.944
800	5	45.1	19.2	5.69	8.655	6.82	1.070
800	7	43.2	18.5	6.57	8.711	6.64	0.974

Specific surface area (BET)

To get a more direct measure of how much internal cracking and porosity the thermal shock treatment created, the specific surface area, pore diameter, and pore volume of the raw sample and of every treated sample were measured using Brunauer–Emmett–Teller (BET) nitrogen adsorption analysis. The pore volume, also called the void volume, is the total volume of empty pore space measured per gram of sample; the pore diameter is the average width of those pores, calculated from the surface area and pore volume as $4V/A$. Table 3 and Figure 14 show the results.

Table 3 Specific surface area, average pore diameter, and pore (void) volume (BET) of the raw sample and treated samples.

Temp. (°C)	Time (min)	Surface area (m^2/g)	Pore diam. (nm)	Pore volume (cm^3/g)
Raw	–	3.40	13.39	0.0107
600	2.5	6.36	10.54	0.0158
600	5	6.06	11.21	0.0158
600	7	6.39	12.61	0.0154
700	2.5	5.92	12.48	0.0172
700	5	5.90	12.40	0.0125
700	7	5.33	13.36	0.0136
800	2.5	4.98	15.96	0.0155
800	5	5.46	15.08	0.0191
800	7	6.57	12.50	0.0144

Bond Work Index

The Bond Work Index (Wi) is an empirical measure of how resistant an ore is to grinding, and it is the standard metric used across the mineral processing industry to estimate comminution energy requirements. It comes from Bond's third theory of comminution [5], which is not a fundamental physical law but an empirical equation fitted to observed grinding data: it proposes that the specific grinding energy needed to reduce an ore from a feed size to a product size is proportional to the difference between the reciprocal square roots of those two sizes. This empirical relationship, Bond's general comminution equation, relates the specific grinding energy

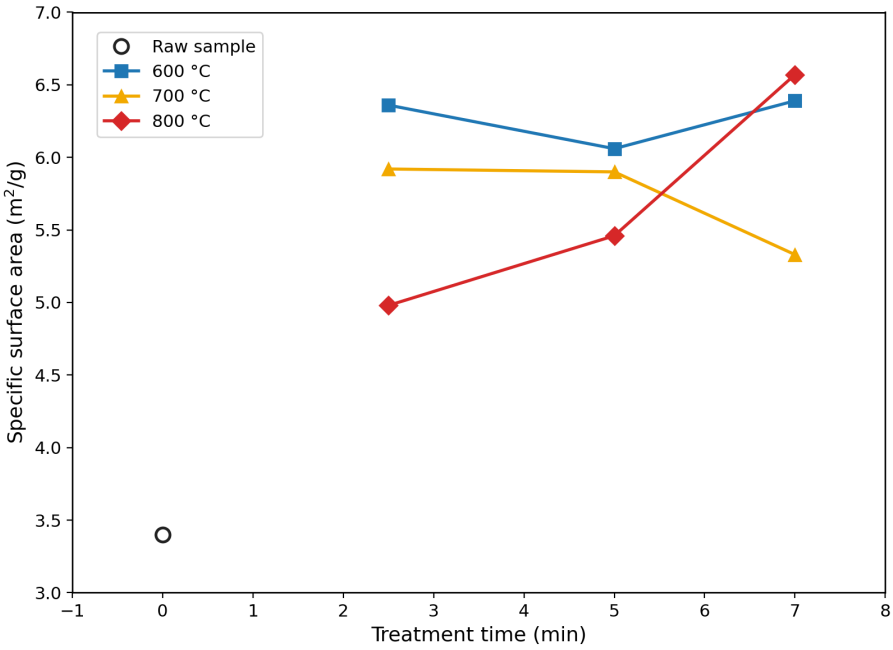


Figure 14 Specific surface area (BET) of samples treated at 600 °C, 700 °C, and 800 °C as a function of treatment time, compared with the raw sample.

input E (kWh/ton) to the ore's Work Index W_i and the 80% passing sizes of the feed (F) and product (P) streams, in micrometers:

$$E = 10\, W_i \left(\frac{1}{\sqrt{P}} - \frac{1}{\sqrt{F}} \right) \tag{1}$$

To determine how thermal treatment changed the grindability of the ore, this study did not attempt to measure W_i directly for every sample. Instead, it used a comparative (relative) form of Eq. (1), a standard approach in grindability testing [5] in which a reference ore of known Work Index is ground under the same conditions as the test ore, and the two specific energies are assumed equal because both are ground for the same fixed time in the same mill. Setting Eq. (1) equal for the reference and test streams and solving for the test ore's Work Index, $W_{i,t}$, gives:

$$W_{i,t} = W_{i,x} \frac{\left| \frac{10}{\sqrt{P_r}} - \frac{10}{\sqrt{F_r}} \right|}{\left| \frac{10}{\sqrt{P_t}} - \frac{10}{\sqrt{F_t}} \right|} \tag{2}$$

Where $W_{i,x}$ is the reference Work Index (kWh/ton), and $W_{i,t}$ is the test ore Work Index for the treated sample. P_r and F_r are the measured 80% passing sizes of the reference product and feed streams, respectively, and P_t and F_t are the corresponding 80% passing sizes for the test (treated) ore product and feed streams. In this study, $W_{i,x}$ was taken as 16.1 kWh/ton, the reference value for this gold ore, with F_r fixed at 8000 μm and P_r fixed at 75 μm. $W_{i,t}$ was then calculated from Eq. (2) for the raw sample and for every treated sample, using each sample's measured F_t and P_t. A lower calculated $W_{i,t}$ therefore indicates that a sample requires less energy to grind, i.e. that the thermal shock treatment improved grindability relative to the untreated ore.

Figure 15 shows how the calculated Work Index (Wi,t) of the treated ore changes with treatment time at each temperature, compared with the raw sample.

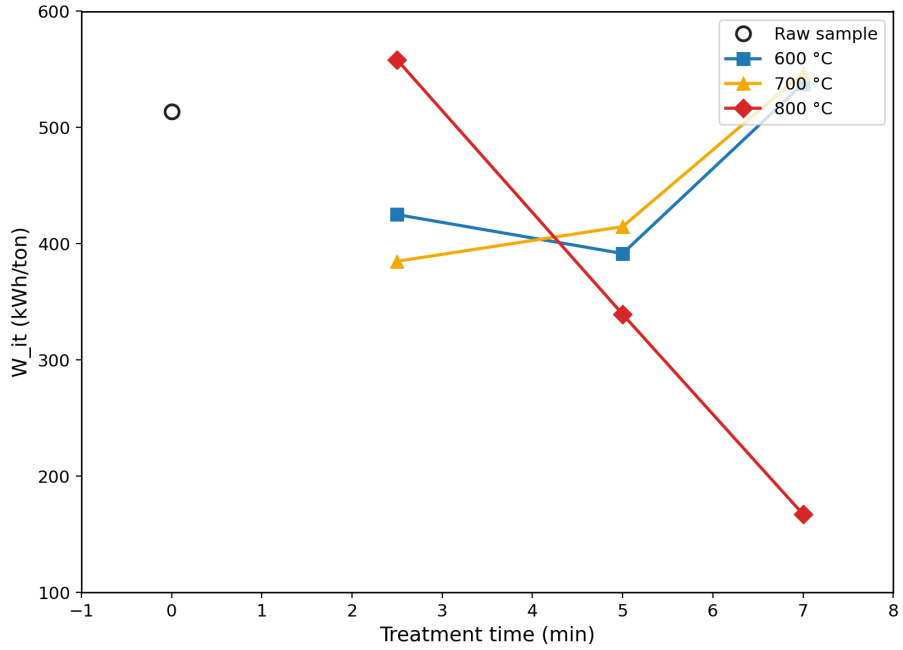


Figure 15 Work Index (Wi,t) of samples treated at 600 °C, 700 °C, and 800 °C as a function of treatment time, compared with the raw sample.

Principal Component Analysis (PCA)

To see how all of the measured quantities in this study relate to one another at once, rather than two at a time, a Principal Component Analysis (PCA) was carried out on the treated samples, using treatment temperature (T), treatment time (t), the XRF composition (SiO_2, Al_2O_3, Fe_2O_3, CaO, MgO, SO_3), the ground particle sizes (D_{80}, D_{50}, D_{10}), the Bond Work Index (labeled BW), and the BET results (specific surface area, pore diameter Pd, and void volume Vvoid) as input variables. PCA reduces this large set of correlated variables down to a small number of new axes, called principal components, chosen so that each one captures as much of the remaining variation in the data as possible. Figure 16 shows the resulting loading plots for the first three components: panel (a) plots PC1 against PC2, and panel (b) plots PC1 against PC3. On these plots, variables whose arrows point in a similar direction rise and fall together across the samples (a direct, positive relationship); variables whose arrows point in opposite directions move against each other (an inverse, negative relationship); and variables at roughly a right angle to one another vary independently. Together, the first three components account for about 79% of the total variation in the dataset (PC1: 41.81%, PC2: 20.96%, PC3: 16.49%).

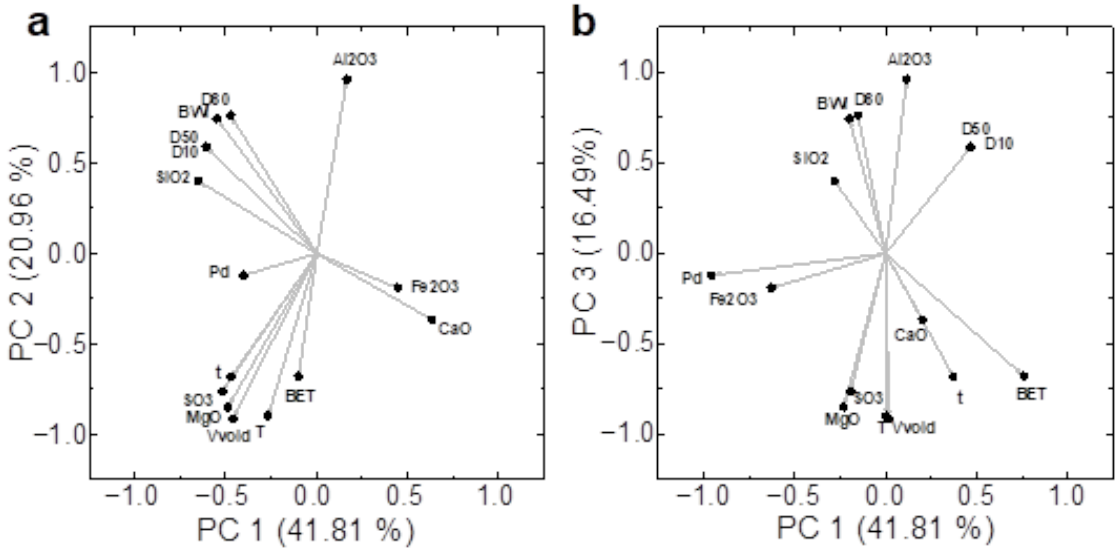


Figure 16 Principal Component Analysis (PCA) loading plots for the treated samples. (a) PC1 vs. PC2. (b) PC1 vs. PC3. T and t are treatment temperature and time; D_{80}, D_{50}, and D_{10} are ground particle sizes; BW is the Bond Work Index; BET, Pd, and Vvoid are the specific surface area, pore diameter, and void (pore) volume; the remaining labels are the XRF oxide compositions.

5 Discussion

Interpretation of Mass Loss

Mass loss increases with temperature, as expected: higher temperatures cause more mineral decomposition and gas release. This mirrors the two-step TGA profile of the raw ore (Figure 7a), where essentially all of the accessible weight loss also occurs between 600 °C and 850 °C. Because heating is driven by radiative flux at the sample surface, the outer layers heat fastest, and a steep radial thermal gradient develops as heat diffuses inward by conduction. At 800 °C, mass loss peaks at 2.5 and 5 min, then drops slightly at 7.5 min, suggesting most decomposition finishes within the first few minutes at this temperature.

Chemical composition

Table 2 tells the same story from a different angle. MgO rises from 13.3% in the raw sample to roughly 15–19% in treated samples, fitting the mass-loss data: heating breaks down magnesium carbonate and drives off CO_2, leaving a solid richer in MgO. Al_2O_3 falls in most treated samples, from 8.31% to about 6.6–8.0% at 600–800 °C, consistent with chlorite breakdown. These changes support both carbonate decomposition and chlorite breakdown as drivers of the observed mass loss and cracking.

Specific surface area (BET)

Table 3 and Figure 14 give a more direct look at the internal cracking and porosity created. Every treated sample has a higher surface area than the raw sample (3.40 m^2/g), confirming that thermal shock opens up internal surface area even at 600 °C, where mass loss alone suggested only a modest effect. At 600 °C, surface area stays roughly flat with time (6.36, 6.06, 6.39 m^2/g), matching its small, inconsistent grindability benefit. At 700 °C, surface area falls with longer exposure (5.92, 5.90, 5.33 m^2/g), pointing to sintering or pore closure. At 800 °C, the trend reverses: surface area is lowest at 2.5 min (4.98 m^2/g) and rises at 5 and 7 min (5.46 and 6.57 m^2/g), matching the sharp drop in $W_{i,t}$ with time described below.

Pore diameter and pore volume add more detail. Every treated sample has a higher pore volume than the raw sample (0.0107 cm^3/g), an independent confirmation of increased void space. Pore diameter is calculated as $4V/A$, so for a given pore volume, more surface area means narrower pores. This shows clearly at 800 °C, where pore diameter falls from 15.96 nm at 2.5 min to 12.50 nm at 7 min, the mirror image of the rising surface area: the pore network is getting finer, not just larger, consistent with growing microcracks rather than a few large voids. The 700 °C samples show the same relationship in reverse: pore volume peaks early (0.0172 cm^3/g at 2.5 min) then falls, while pore diameter drifts back up, both pointing to partial pore closure. At 600 °C, pore volume stays roughly flat and above the raw sample throughout (0.0158, 0.0158, 0.0154 cm^3/g), consistent with the small amount of cracking already implied by the surface-area data.

Grindability at 600 °C

The 2.5 and 5 min treatments show a small grindability improvement: their curves sit slightly above the raw sample in both size ranges. The 7 min treatment performs slightly worse than the raw sample. This suggests a short exposure at 600 °C causes some useful cracking, while a longer exposure may sinter the particle surfaces together, making them harder to break.

Grindability at 700 °C and 800 °C

At 700 °C, all three exposure times show clear improvement over the raw sample. The 2.5 and 5 min treatments perform similarly, while 7.5 min shows a smaller improvement, again suggesting diminishing returns from longer exposure.

At 800 °C, the 5 and 7.5 min treatments give the strongest improvement of all conditions tested, with 7.5 min showing the highest cumulative passing values overall. This is somewhat different from what the mass loss data alone would suggest: the 7.5 min sample lost less mass (15.0%) than the 2.5 and 5 min samples (17.5% each), yet showed the best grindability. Mass loss alone is therefore not a perfect predictor of grindability; internal cracking and structural weakening likely matter more than the total material lost.

Work Index (Wi,t)

The $W_{i,t}$ values in Figure 15 mostly agree with the particle-size grindability trends, and the BET data in Table 3 and Figure 14 help explain why. At 800 °C, $W_{i,t}$ drops sharply with time, from 558 kWh/ton at 2.5 min, higher than the raw sample's 514 kWh/ton, down to 167 kWh/ton at 7 min. This tracks the rising surface area at 800 °C (4.98, 5.46, 6.57 m^2/g): more surface area means less grinding energy is needed. The high $W_{i,t}$ at 2.5 min matches the earlier finding that this condition underperforms despite its high mass loss: decomposition has started but the cracks have not yet fully developed.

At 700 °C, $W_{i,t}$ falls at 2.5 and 5 min but rises above the raw sample's value at 7 min, mirroring the falling surface area at this temperature (5.92, 5.90, 5.33 m^2/g), consistent with sintering or pore closure.

At 600 °C, $W_{i,t}$ shows a similar rebound at 7 min, but the BET data do not tell as clean a story: surface area stays roughly flat (6.36, 6.06, 6.39 m^2/g) rather than falling. The worse grindability at 7 min may involve more localized effects, such as surface necking, that bulk BET measurement does not capture. This gap is also likely because $W_{i,t}$ is calculated from only two points on the particle size curve, making it more sensitive to small shifts than the full cumulative passing curves.

The 800 °C/2.5 min sample remains an exception: its curve sits close to, or below, the raw sample despite one of the highest mass losses (17.5%). A plausible explanation is that a very short exposure triggers decomposition but not enough time for the resulting cracks to develop

before cooling.

Principal Component Analysis (PCA)

The PCA loading plots in Figure 16 pull together nearly every result above into one picture, and largely confirm the temperature-by-temperature analysis. The Bond Work Index (BW) and the ground particle sizes (D_{80}, D_{50}, D_{10}) cluster tightly and point in the same direction in both panels: a coarser ground product directly means a higher, worse Work Index, so PCA groups them as one positively correlated bundle. SiO_2 sits close to this cluster, meaning samples with more residual SiO_2 tend to be harder to grind, consistent with quartz being the inert phase left behind once carbonate and clay minerals decompose.

On the opposite side, treatment time (t), MgO, SO_3, and void volume (Vvoid) cluster tightly and point in a clearly different direction from the BW/D-value cluster, in both panels: an inverse relationship. As treatment time increases and the ore loses more carbonate as CO_2, raising relative MgO and SO_3 and opening more void volume, the Bond Work Index and particle sizes fall, i.e. the ore gets easier to grind. This matches the mechanism already described for mass loss, chemical composition, and BET, and it is reassuring to see PCA recover the same story from all variables at once. BET surface area sits close to this cluster in panel (a) but separates along PC3 in panel (b), fitting the earlier observation that surface area does not always move in lockstep with the other decomposition markers.

Pore diameter (Pd) and Fe_2O_3 cluster together and point away from the time/MgO/SO_3/void-volume cluster, most clearly in panel (b), consistent with the $4V/A$ relationship: more surface area packed into the same pore volume means narrower pores. Al_2O_3 stands apart from every other variable, loading almost entirely on PC2 in panel (a) and PC3 in panel (b), staying near zero on PC1 in both. Since Al_2O_3 tracks chlorite breakdown, this suggests it varies largely independently of the main carbonate-decomposition axis that PC1 represents, as the two are different chemical reactions. CaO sits between the main clusters in both panels without aligning clearly with either, matching the earlier finding that CaO follows no clear monotonic trend.

Overall, the PCA does not contradict the rest of the analysis. Its main value is confirming, from all variables at once, that a single underlying factor, the severity of thermal decomposition, drives most of the variation in this dataset, with Al_2O_3/chlorite breakdown and the pore-diameter/surface-area relationship appearing as secondary, largely independent directions of variation.

6 Limitations and Future Work

- **Simulated vs. real sunlight.** This study used a high-flux solar simulator rather than real sunlight. The longer-term goal is to use real sunlight, focused with mirrors or lenses, to heat the ore directly at a mine site. Field trials would confirm the same heating rates and grindability improvements can be reproduced outdoors, where solar flux varies with weather and time of day.
- **The 800 °C/2.5 min anomaly is not fully explained.** This condition combined a high mass loss with below-average grindability, contradicting the general trend. Follow-up testing with additional short exposure times, paired with microstructural imaging, would help confirm whether this reflects insufficient crack development time or a small-sample artifact.
- **Mass loss alone is not a reliable predictor of grindability.** At 800 °C, the sample with the lowest mass loss showed the best grindability, while higher mass-loss samples underperformed. Future work should pair mass-loss and XRF/XRD measurements with direct

microcrack quantification, such as micro-CT imaging, to better isolate the structural mechanisms driving grindability improvements.

- **Power was the controlled variable, not temperature.** The solar simulator can only be set to a fixed input power; it has no direct temperature control. The nominal treatment temperatures reported here resulted from running the simulator at a given power for a given time, so two samples at the same power setting are not guaranteed to reach exactly the same temperature. Future work should add closed-loop temperature control that adjusts power in real time to hold a target temperature.
- **Temperature measurement was not fully accurate.** The thermocouple measures temperature at a single contact point and can be affected by imperfect contact, thermal lag, and interference from the simulator's radiative flux. Reported temperatures should be treated as approximate, which may partly explain the 800 °C/2.5 min anomaly. Future work should use a non-contact method, such as an infrared pyrometer, to verify or replace the thermocouple readings.
- **Downstream processing was not evaluated.** This study only assessed comminution energy, not how the treated ore behaves in downstream steps such as cyanide leaching. Targeted leaching tests would confirm whether the mineralogical changes observed here translate into real gains for gold recovery.

7 Conclusion

This study shows that thermal shock from a concentrated solar simulator meaningfully improves the grindability of gold ore, mirroring benefits previously reported for furnace-based thermal shock. Mass loss, driven by carbonate decomposition and chlorite dehydroxylation, increased with temperature, reaching up to 16.7% at 800 °C. Grindability improved most at 700 and 800 °C, with the Bond Work Index at 800 °C falling from 558 kWh/ton at 2.5 min to 167 kWh/ton at longer exposure, a reduction of nearly 70% relative to the raw sample. Grinding energy is not explained by mass loss alone, indicating that internal microcracking, not simple decomposition, mainly drives improved grindability. The main takeaway is that radiative solar heating closes an open gap in the thermal shock literature: it can reproduce the same grinding-energy savings previously reported only for furnace thermal shock, while replacing grid electricity with concentrated sunlight.

Acknowledgments

The author sincerely thanks Prof. Bassam Dally and Dr. Ali Alkadhem for their guidance, feedback, and support throughout this project, and the wider ReSET Group at KAUST for their help and collaboration. The author also gratefully acknowledges the King Abdullah City for Atomic and Renewable Energy (K.A.CARE) for its financial support of KAUST Academy, and KAUST Academy itself for the opportunity to carry out this project. Finally, the author thanks Maaden for sponsoring the group and its research.

References

[1] Fuerstenau, D. W. and Abouzeid, A.-Z. M. (2002). The energy efficiency of ball milling in comminution. *International Journal of Mineral Processing*, 67(1-4):161–185. https://doi.org/10.1016/S0301-7516(02)00039-X

[2] Somani, A., Nandi, T. K., Pal, S. K., and Majumder, A. K. (2017). Pre-treatment of rocks prior to comminution – a critical review of present practices. *International Journal of Mining Science and Technology*, 27(2):339–348. https://doi.org/10.1016/j.ijmst.2017.01.013

[3] Rodriguez-Navarro, C., Kudlacz, K., and Ruiz-Agudo, E. (2012). The mechanism of thermal decomposition of dolomite: New insights from 2D-XRD and TEM analyses. *American Mineralogist*, 97(1):38–51. https://doi.org/10.2138/am.2011.3813

[4] Ababneh, H., Lopez Aguirre, A., Alkadhem, A. M., and Dally, B. (2026). Reducing comminution energy of gold ores through thermal shock treatment. *Mineral Processing and Extractive Metallurgy Review*. https://doi.org/10.1080/08827508.2026.2680439

[5] Bond, F. C. (1952). The third theory of comminution. *Transactions of the American Institute of Mining, Metallurgical, and Petroleum Engineers*, 193:484–494.